COMPUTATIONAL FLUID DYNAMICS SIMULATIONS OF VARIANT DESIGNS OF THE BIPOLAR PLATE FLOW FIELDS FOR PROTON EXCHANGE MEMBRANE FUEL CELL

Channa Keshava Naik N[1], Aneesh Jose[2], Rudra Naik[3], Sudesh Bekal[4], Sameer G[4], Abdulrajak Buradi[5], Addisu Frinjo Emma[6], and Anil Kumar H M[7]

[1]BGS College of Engineering and Technology
[2]Visvesvaraya Technological University Consortium
[3]BMS College of Engineering Department of Mechanical Engineering
[4]NMAM Institute of Technology Department of Mechanical Engineering
[5]NITTE Meenakshi Institute of Technology Department of Mechanical Engineering
[6]Dilla University
[7]Ballari Institute of Technology and Management

April 28, 2024

Abstract

Bipolar plates in the fuel cells are mechanical components chiefly responsible for power variation and even distribution of fuel and oxidant at the membrane exchange assembly. To ensure the fuel cell optimal performance and longevity of the membrane the flow field pressures need to be in the optimum range. In this study, a combination of existing and new designs of bipolar plate flow Fields for 100 × 100mm area membrane exchange assembly Size have been modelled and studied with the help of computational fluid dynamics. A total of six variant designs have been analyzed. An attempt is made to understand the most efficient channel design which results in a good flow field & low-pressure drop. The simulation studies indicate that the serpentine channel with two channels-opposite inlets-outlets provides the most uniform pressure drop and the best fuel distribution and is 10% better than the serpentine conventional single-channel bipolar plate Flow fields.

INTRODUCTION

Fuel cells convert energy in fuels such as hydrogen or methanol into electrical work without producing any harmful exhaust emissions, their exhaust by-product are either steam or water. PEM (proton exchange membrane) Fuel cell consists of Bipolar plates, Membrane exchange assembly (MEA), current collector, and end plates. The MEA consists of the membrane and the catalysts. The catalyst thickness is different on the cathode and anode sides. The membrane allows only protons to flow through it and the electrons are forced in through an external circuit, the redox reaction from the reaction on the cathode and anode sides together completes the reaction to produce electricity and meet the electrical requirements. Fig. 1 illustrates parts of the PEM fuel cell with bipolar plates juxtaposed with collector plates and a membrane exchange assembly consisting of an anode and cathode on either side of the membrane also in the side view the cross-section of one such channel shows the channel area, Gas diffusion layer (GDL), and membrane can be seen. The figure also gives the terminology of the bipolar plate consisting of the flow area and ribs of the flow field. The reaction occurring within the Fuel cell layers can be summarized as follows:

Reactions at cathode site: O2 + 2H2O + 4e^{-} - 4OH^{-}

Reactions at Anode site: $2H2 + 4OH^{-} - 4H2O + 4e^{-}$

Net Cell Reactions: $2H2 + O2 - 2H2O$

The Bipolar plates have channels through which gases flow and feed the gas diffusion layer. Channel width is the distance between two adjacent flow channels and rib width is the width of the flow channel. When the rib width is more than that of the channel width, the contact between fuel and membrane increases.[1-2] Additionally, Bipolar plates provide passage for the evacuation of condensed water which otherwise would clog the fuel cell and render it inefficient. Also, the Bipolar plates provide a pathway for the movement of electrons from the Anode to the cathode and provide a medium for heat transfer to the surroundings. In the absence of a genuine medium for heat transfer, there would be thermal stresses created which in due course of time would rupture the electrolyte membrane.[3-4]

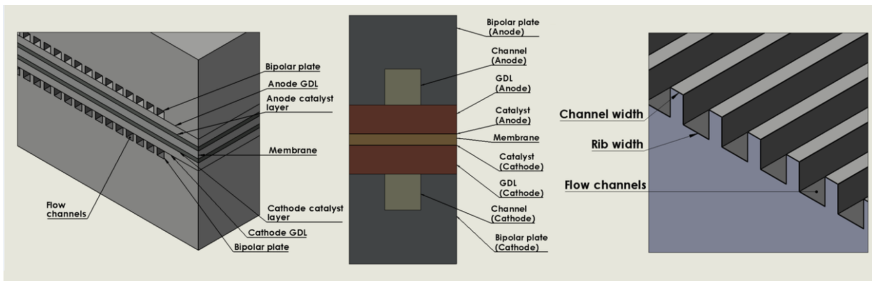

Fig.-1: PEM Fuel cell parts, channel widths, rib widths & Flow area for a single cell plate

Extensive work has been carried out by researchers to improve the efficiency of fuel cells and optimize the various components of the fuel cell. The Bipolar plate channel design plays a major role in ensuring the uniform distribution of gases and thereby affects the performance of the fuel cell.[5-8] Fuel cell efficiency amounted to 72.4% and exergy efficiency to 85.22% for a fuel cell at a pressure of 0.5 bar with a flow rate of 0.21LPM, the findings also reported that the PEM fuel cell efficiency can be enhanced by optimizing the pressures, fuel flow rates and use of efficient designs of bipolar plates.[9-12] By selection of appropriate flow field plates (FFP) design pressure drop in the channels can be reduced. Poorly designed FFPs can result in uneven reactant distribution on the channel and subsequent water condensation on the cathode side and water droplet accumulation which clogs the channel or allows moisture layer deposit on the GDL.[13-16] Many types of research indicate that miniature changes in the BP design can lead to changes in the power density of the Fuel cell up to a maximum value of 300%.[2]

The conventional single serpentine FFPs are the most widely used however research has been going on in establishing the most efficient channels to be used in Bipolar plates.[17-20] There are many variations to basic serpentine design such as single-channel serpentine, multi-channel serpentine, mirrored serpentine, Converging and diverging serpentine with guiding plates, and serpentine with water holes.[21-22] The interdigitated design was developed mainly to ensure forced passage of reactants and products and reduce concentration polarization losses thereby producing better efficiency, however, there is a trade-off to be paid in the form of higher-pressure losses. Pin-type Bipolar plates have many advantages such as better flow, uniform pressure drops, etc., however, due to the excessive convective forces, the MEA may be damaged over a long run of time.[23-25] Also Pin-type bipolar plates have produced flat current densities compared to that of interdigitated or serpentine plates and have resulted in 25% higher power density.[26-27] The modifications of the conventional serpentine channel into Z-type and U-type parallel channel configurations by segmentations were investigated, and they showed much-improved flow quality of gases through them.[28-29]The analysis carried out on 4-step serpentine and pin geometries indicated the good distribution of the reactants. The current density curve for these designs is found to be flatter compared to parallel or interdigitated and hence yielded higher power values.[26] The mesh type design has been found to give low-pressure drop due to low hydrodynamic resistance offered by interconnected mesh areas; however, the mesh type having many routes for the fluid flow from inlet to outlet was found to have low resistivity and high flow rates at the diagonals. Flooding issues were also observed with mesh-type bipolar plates at prolonged usage.[26,28,30]

The design of bipolar plates has also been inspired by nature having particular arrangements of branches of leaves and vines. The study reporting leaf-inspired FFP designs such as i) pinnate venation and dichotomous angles and ii) parallel with two tapered channels, indicated constructal theory to numerically prognosticated the mean current density of the 3D tree-like pattern PEM fuel cell to be higher than conventional serpentine FFP.[31-32] A study on Bipolar plates with porous inserts in between the pins ensured a better homogenous reactant distribution capacity however with the disadvantage of inserts increasing pressure losses.[33-34] The computational fluid dynamics (CFD) model is highly useful in modelling processes. CFD model helps in investigations in the area of flow analysis, pressure differences, transport, and electrochemical phenomena in fuel cells. [35-37]

The literature indicates a gap in achieving an ideal FFPs Bipolar plate for fuel cells that can manage effectiveness in fuel distribution over MEA with good water management and negligible pressure drops. These issues are addressed in this work by using combinations of designs from serpentine and providing more than one flow field channel on the plate. The pressure drops of gas flow across the channel are analyzed by using CFD simulations through licensed ANSYS Fluent software to study the effectiveness of the design considered in this work.

BIPOLAR PLATE FLOW FIELD DESIGNS

For the fuel cell to work efficiently at an even pressure drop across the Flow field area is a basic necessity. Ideally, the pressure of the gas should remain the same at the inlet and outlet of the bipolar plate flow fields, however, this is very uncommon due to variations across channel length. The novelty has been achieved by providing more than one channel on the same plate and also changing the directions of flow in adjacent channels this was achieved by providing many inlet and outlet ports. The novel designs are expected to make gas distribution more uniform and limit pressure loss by suitable arrangement of the gas flow path, location, and number of inlet outlets. In all, a total of six designs have been analyzed using ANSYS CFD for pressure variations. Pin-type Bipolar plate which had been studied earlier mostly had fewer projections; however, in this work, the modified bipolar plate with a large number of circular pins have been used and bipolar plates with rectangular pins have been studied. The designs considered here are; i) Serpentine Single Channel (BP1) ii) Serpentine 3×3 single channel (BP2) iii) Serpentine 3×3 double channel with two common inlets (BP3) iv) Serpentine 3×3 double channel with opposite inlets (BP4) v) Pin type bipolar plate with circular extrusions (BP5) and vi) Pin type bipolar plate with rectangular extrusions (BP6). The 3D geometry of various flow fields was created with basic CAD software, all the channel configurations are made using the sweep feature and the linear sketch pattern feature available on the software. A rectangular cross-section of 1×1 mm is made normal to the channel path and the cross-section is swept cut throughout the channel pattern to obtain the final model.

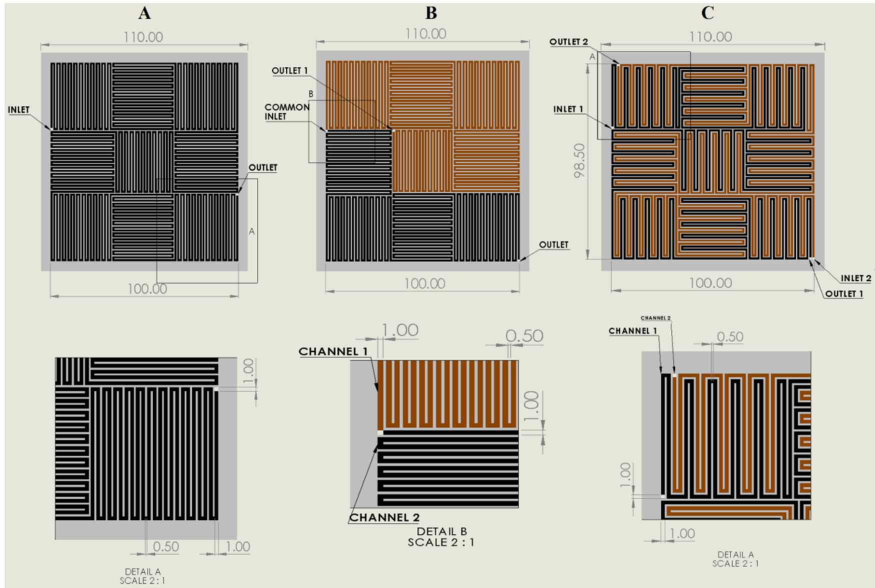

Fig.-2: BP2, BP3 & BP4. Fig. A BP2-serpentine 3 × 3 single channel - bipolar plate flow field. Fig. B BP3-serpentine 3 × 3 double channel with common inlets-bipolar plate flow field. Fig. C BP4-serpentine 3 × 3 double channel with opposite inlets-bipolar plate flow field. Enlarged images in the sections below give the dimensions of the rib and channel width.

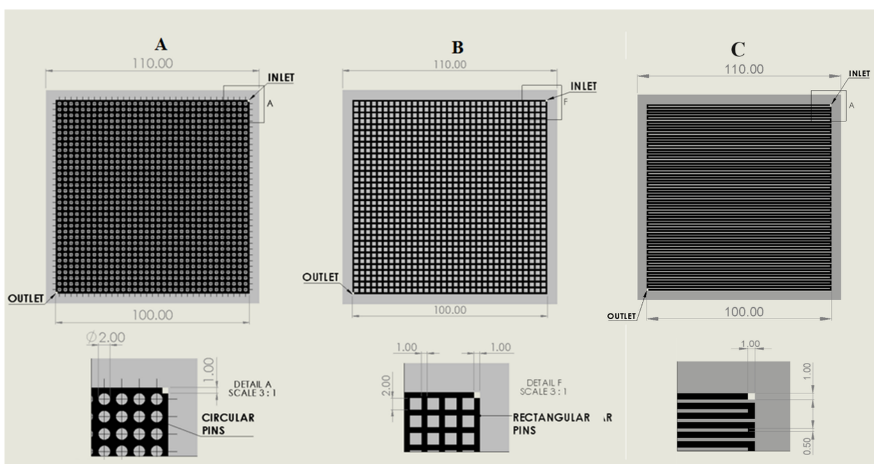

Fig.-3: BP5, BP6 & BP1. Fig. A BP5-pin type bipolar plate flow field design with circular extrusions & Fig. B BP6-pin type bipolar plate flow field design with rectangular extrusion. Fig. C BP1. Serpentine single channel - bipolar plate flow field design. The enlarged image of the sections below gives the dimension of the rib and channel widths of corresponding flow fields.

These designs have been considered for the study of variation in pressure and pressure drops using CFD simulations. Fig. 2 A, B & C & Fig. 3 A B & C show the schematic CAD diagrams of proposed bipolar plates. All the Bipolar plates mentioned here have uniform channel widths and depths. The channel width to rib width ratio has been maintained at 2:1 which is considered to be the most beneficial proportion with a rib width of 0.5mm.[38]

Table-1: Flow field design parameters for the six bipolar plates flow fields BP1, BP2, BP3, BP4, BP5 & BP6.

S. No	Channel Design	Active flow volume	Channel Depth (mm)	No of Channels* /pins#	Channel to rib width	No of Bends
1.	BP1	6752	1	67*	2:1	66
2.	BP2	6752	1	198*	2:1	184
3.	BP3	6760	1	198*	2:1	107
4.	BP4	6668	1	198*	2:1	195
5.	BP5	6579	1	1089 #	1:1	NA
6.	BP6	5644	1	1089#	2:1	NA

The GDL area (area of contact for fuel and catalysts also the MEA area) for the Bipolar plates is 100×100 mm^2. The active surface area and active flow volume are the same and no channels are given in Table 1. Fig. 2A shows the CAD diagram for the Serpentine 3×3 single-channel bipolar plate (BP2), the flow takes place through the inlet port through nine sets of channels which creates nine segments in the bipolar plate of which there are four horizontal flow fields and five vertical flow fields. This arrangement is to keep pressure uniform on individual segments. Fig. 2B shows the design for a Serpentine 3×3 double channel with two common inlets (BP3), the double-flow fields are provided in order to have uniform pressure drops throughout the plates when the pressures at one end of the channel decrease simultaneously on the other channel pressure increases due to opposite inlets thereby nullifying the low pressures on the GDL. This design is similar to the previous serpentine single 3×3 channel except for the common inlets and two outlets. Fig. 2C shows the Serpentine 3 × 3 double channels with opposite inlets (BP4); this serpentine design has two exclusive channels and hence two different inlets and outlets have been provided. The channels have opposite inlets and outlets to ensure the supply of rich fuel in all parts of the area equally. The flow takes place through the inlet port through nine sets of channels which creates nine segments in the bipolar plate of which there are four horizontal flow fields and five vertical flow fields.

Fig. 3 gives details of the pin type of bipolar plates. Fig. 3A depicts pin type with circular extrusion whereas Fig. 3B illustrates rectangular extrusions. A magnified view of a section of pins and its dimension is shown below each corresponding diagram. The diameter of the circular and rectangular pins is 2 mm, the center distance between the circular pins is 3 mm and between these pins the gas flow takes place. Fig. 3C shows CAD diagrams of the Serpentine Single Channel bipolar plate (BP1). This channel has been included here for comparison purposes with the other channels. The inlet and outlet are located at the ends of the flow channel diagonally opposite to each other.

CFD SIMULATIONS

CFD simulation was carried out using Licensed ANSYS CFD Fluent with unlimited nodes. The CFD simulations involved the following steps, formulating the flow region, establishing boundary and initial conditions, generating the grid, identifying and establishing the simulation strategy, and finally performing the simulations with the gathering of results. PEM Fuel cells typically operate between 20 $^{\circ}$C and 100 $^{\circ}$C, from 1 to 3 bar pressure. The pressure values for all six Bipolar plates have been simulated in order to arrive at the most suitable bipolar plate with the least pressure drop. Hydrogen gas has been considered as the flowing fluid through the flow fields, the density of hydrogen is 0.08375 kg/m^3 all parameters are considered at NTP. The fluid flow analysis followed the numerical computational method using the principle of the Navier-Stokes equation for viscous models.

The momentum conservation equations are expressed in the x, y, and z directions, for a Newtonian fluid applying the Navier stokes equation

$$\frac{\partial}{\partial t}(\rho \vec{v}) + \nabla$$

$$\frac{\partial}{\partial t}(\rho \vec{v}) + \nabla$$

$$\frac{\partial}{\partial t}(\rho \vec{v}) + \nabla$$

$$\frac{\partial}{\partial t}(\rho \vec{v}) + \nabla$$

$$\frac{\partial}{\partial t}(\rho \vec{v}) + \nabla$$

$$\frac{\partial}{\partial t}(\rho \vec{v}) + \nabla$$

$$\frac{\partial}{\partial t}(\rho \vec{v}) + \nabla$$

$$\frac{\partial}{\partial t}(\rho \vec{v}) + \nabla$$

$$\frac{\partial}{\partial t}(\rho \vec{v}) + \nabla$$

$$\frac{\partial}{\partial t}(\rho \vec{v}) + \nabla$$

$$\frac{\partial}{\partial t}(\rho \vec{v}) + \nabla$$

$$\frac{\partial}{\partial t}(\rho \vec{v}) + \nabla$$

.= +.()+ Eq. (1)

$$\frac{\partial}{\partial t}(\rho \vec{v}) + \nabla$$

$$\frac{\partial}{\partial t}(\rho \vec{v}) + \nabla$$

The stress tensor   is expresses as

$$\frac{\partial u}{\partial t} + \frac{\partial u^2}{\partial x} + \frac{\partial uv}{\partial y} + \frac{\partial uw}{\partial z} = -\frac{1}{\rho}\frac{\partial p}{\partial x} + \nu\left(\frac{\partial^2 u}{\partial x^2} + \frac{\partial^2 u}{\partial y^2} + \frac{\partial^2 u}{\partial z^2}\right)$$

$$\frac{\partial u}{\partial t} + \frac{\partial u^2}{\partial x} + \frac{\partial uv}{\partial y} + \frac{\partial uw}{\partial z} = -\frac{1}{\rho}\frac{\partial p}{\partial x} + \nu\left(\frac{\partial^2 u}{\partial x^2} + \frac{\partial^2 u}{\partial y^2} + \frac{\partial^2 u}{\partial z^2}\right)$$

$$\frac{\partial u}{\partial t} + \frac{\partial u^2}{\partial x} + \frac{\partial uv}{\partial y} + \frac{\partial uw}{\partial z} = -\frac{1}{\rho}\frac{\partial p}{\partial x} + \nu\left(\frac{\partial^2 u}{\partial x^2} + \frac{\partial^2 u}{\partial y^2} + \frac{\partial^2 u}{\partial z^2}\right)$$

$$\frac{\partial u}{\partial t} + \frac{\partial u^2}{\partial x} + \frac{\partial uv}{\partial y} + \frac{\partial uw}{\partial z} = -\frac{1}{\rho}\frac{\partial p}{\partial x} + \nu\left(\frac{\partial^2 u}{\partial x^2} + \frac{\partial^2 u}{\partial y^2} + \frac{\partial^2 u}{\partial z^2}\right)$$

$$\frac{\partial u}{\partial t} + \frac{\partial u^2}{\partial x} + \frac{\partial uv}{\partial y} + \frac{\partial uw}{\partial z} = -\frac{1}{\rho}\frac{\partial p}{\partial x} + \nu\left(\frac{\partial^2 u}{\partial x^2} + \frac{\partial^2 u}{\partial y^2} + \frac{\partial^2 u}{\partial z^2}\right)$$

$$\frac{\partial u}{\partial t} + \frac{\partial u^2}{\partial x} + \frac{\partial uv}{\partial y} + \frac{\partial uw}{\partial z} = -\frac{1}{\rho}\frac{\partial p}{\partial x} + \nu\left(\frac{\partial^2 u}{\partial x^2} + \frac{\partial^2 u}{\partial y^2} + \frac{\partial^2 u}{\partial z^2}\right)$$

Eq. (2)

The mass conservation is given by,

$$\frac{\partial u}{\partial t} + \frac{\partial u^2}{\partial x} + \frac{\partial uv}{\partial y} + \frac{\partial uw}{\partial z} = -\frac{1}{\rho}\frac{\partial p}{\partial x} + \nu\left(\frac{\partial^2 u}{\partial x^2} + \frac{\partial^2 u}{\partial y^2} + \frac{\partial^2 u}{\partial z^2}\right)$$

$$\frac{\partial u}{\partial t} + \frac{\partial u^2}{\partial x} + \frac{\partial uv}{\partial y} + \frac{\partial uw}{\partial z} = -\frac{1}{\rho}\frac{\partial p}{\partial x} + \nu\left(\frac{\partial^2 u}{\partial x^2} + \frac{\partial^2 u}{\partial y^2} + \frac{\partial^2 u}{\partial z^2}\right)$$

Eq. (3)

A dimensionless number (Reynolds number) is applicable in fluid mechanics to specify if the fluid flow across a body is turbulent (>4000) or laminar (<2000).

$$\frac{\partial u}{\partial t} + \frac{\partial u^2}{\partial x} + \frac{\partial uv}{\partial y} + \frac{\partial uw}{\partial z} = -\frac{1}{\rho}\frac{\partial p}{\partial x} + \nu\left(\frac{\partial^2 u}{\partial x^2} + \frac{\partial^2 u}{\partial y^2} + \frac{\partial^2 u}{\partial z^2}\right)$$

$$\frac{\partial u}{\partial t} + \frac{\partial u^2}{\partial x} + \frac{\partial uv}{\partial y} + \frac{\partial uw}{\partial z} = -\frac{1}{\rho}\frac{\partial p}{\partial x} + \nu\left(\frac{\partial^2 u}{\partial x^2} + \frac{\partial^2 u}{\partial y^2} + \frac{\partial^2 u}{\partial z^2}\right)$$

Re =

Eq. (4)

$$\frac{\partial u}{\partial t} + \frac{\partial u^2}{\partial x} + \frac{\partial uv}{\partial y} + \frac{\partial uw}{\partial z} = -\frac{1}{\rho}\frac{\partial p}{\partial x} + \nu\left(\frac{\partial^2 u}{\partial x^2} + \frac{\partial^2 u}{\partial y^2} + \frac{\partial^2 u}{\partial z^2}\right)$$

$$\frac{\partial u}{\partial t} + \frac{\partial u^2}{\partial x} + \frac{\partial uv}{\partial y} + \frac{\partial uw}{\partial z} = -\frac{1}{\rho}\frac{\partial p}{\partial x} + \nu\left(\frac{\partial^2 u}{\partial x^2} + \frac{\partial^2 u}{\partial y^2} + \frac{\partial^2 u}{\partial z^2}\right)$$

$$\frac{\partial u}{\partial t} + \frac{\partial u^2}{\partial x} + \frac{\partial uv}{\partial y} + \frac{\partial uw}{\partial z} = -\frac{1}{\rho}\frac{\partial p}{\partial x} + \nu\left(\frac{\partial^2 u}{\partial x^2} + \frac{\partial^2 u}{\partial y^2} + \frac{\partial^2 u}{\partial z^2}\right)$$

$$\frac{\partial u}{\partial t} + \frac{\partial u^2}{\partial x} + \frac{\partial uv}{\partial y} + \frac{\partial uw}{\partial z} = -\frac{1}{\rho}\frac{\partial p}{\partial x} + \nu\left(\frac{\partial^2 u}{\partial x^2} + \frac{\partial^2 u}{\partial y^2} + \frac{\partial^2 u}{\partial z^2}\right)$$

where ρ gives the fluid density (kg/m^3) V is the flow velocity (m/s),

is the fluid viscosity (kg/ms and D_{ch} is the characteristic length (m)

The values of nodes and mesh generated for BP1 to BP6 flow fields are found in Table 2. The graph of the grid independence test which has been basis for identifying the ideal number of mesh for BP1 is given in Fig. 4. Skewness gives the details of mesh shape accuracy and needs to be maintained below 0.8. The maximum skewness was maintained below 0.4 in all cases. The details of the mesh generated for all six flow fields are given in Table 2. The time for convergence on a 64GB RAM i7 processor was found to be 90 Minutes for a mesh element size of 0.1mm.

Table-2: Details of Mesh generated during pre-possessing

S. No	Channel design	No of elements	No of nodes	Average skewness	Average aspect ratio
	BP1	2,22,26,009	2,38,20,614	0.24608	4.7132
	BP2	3,81,53,861	3,00,36,205	0.45873	4.9967
	BP3	2,84,17,113	2,38,20,615	0.38843	26.491
	BP4	1,17,67,805	1,07,67,930	0.30532	9.1751
	BP5	3,97,21,145	2,38,20,616	0.47286	6.4663
	BP6	3,61,44,822	3,41,89,629	0.08914	1.3937

$$\frac{\partial u}{\partial t}+\frac{\partial u^2}{\partial x}+\frac{\partial uv}{\partial y}+\frac{\partial uw}{\partial z}=-\frac{1}{\rho}\frac{\partial p}{\partial x}+\nu\left(\frac{\partial^2 u}{\partial x^2}+\frac{\partial^2 u}{\partial y^2}+\frac{\partial^2 u}{\partial z^2}\right)$$

Fig.-4: Grid independence test for the single serpentine channel.

RESULTS AND DISCUSSIONS

Comparison of pressure distribution for BP1 to BP6 Bipolar plate flow fields are made with the results of single-channel serpentine which has been chosen as the basis. Fig. 5,6,7,8,9 &10 presents the simulations of the pressure distribution of all six bipolar plates. In each of these figures, Fig. A. represents the pressure variations across the channels and Fig. B represents the pressure distribution on a cross-section at the outlet. For a double channel, additional figures represent the cross section the pressure distribution on two channels. All the channel designs are simulated for two inlet gauge pressures of 101325 Pa (1 Bar) and 150000 Pa (1.5 Bar). The pressure drops for all the six channels have been analyzed and its details of inlet pressure, outlet pressure and pressure at the centerline of the Flow field are provided in the table 3. BP3 and BP4 have two adjacent channels, their pressure details across adjacent channels have been provided. The novel BP4 has two inlets and outlets therefore average pressures have been considered at each section. From table 3 following observations are made; for both serpentines and pin flow fields as the inlet pressure increases from 1 bar to 1.5 bar the pressure at the outlet decreases it may even reach below zero-gauge pressures indicating a negative trend at the outlet.

Table-3: Pressure details from CFD simulations at different sections of the Flow fields for BP1 to BP6 at two pressures 101325 Pa & 151987.5 Pa

S. No	Channel Designs	Inlet pressure (Pa)	Maximum pressure inside channel (Pa)	Maximum pressure inside channel (Pa)	Outlet pressure (Pa)	Outlet pressure (Pa)	Centreline Pressure (Pa)	Centrel Pressur (Pa)

BP1	101325	101117	101117	0.0526	0.0526	49170	49170
	151987.5	151601	151601	-0.121	-0.121	52120	52120
BP2	101325	101220	101220	0.0518	0.0518	49550	49550
	151987.5	151800	151800	- 0.009576	- 0.009576	52523	52523
BP3	101325	100608	100608	0.203	0.168	12000	86000
	151987.5	151042	151042	0.189	0.043	12720	91160
BP4	101325	101057	101064	0.375	0.344	49300	49400
	151987.5	151531	151541	0.916	0.279	52258	52364
BP5	101325	87868.8	87868.8	-3.266	-3.266	- 3.716	- 3.716
	151987.5	137329	137329	-15.09	-15.09	-3.016	-3.016
BP6	101325	88987	88987	9.851	9.851	2.37	2.37
	151987.5	133270	133270	20.76	20.76	2.51	2.51

Fig. 5 provides information about the BP1 single serpentine channel, which is used for comparison purposes with other flow field plates. The pressure drop is uniformly reduced from the inlet to the outlet. Fig. 5A shows the pressure across the channel length, while Fig. 5B displays the pressure distribution across the cross-section of the channel outlet. The pressure drops occurring at various channel lengths are represented by different colored sections. The maximum pressure of 101117 Pa can be found at the inlet on the red-colored regions. In the straight portion, pressure drops are minimal on average, whereas the pressure drops in the bends are high on average. The decrease of pressure is gradual along the length of the channels, with the maximum pressure indicated in the red-colored areas at the inlet, which are approximately 25% of the total flow area, while the minimum pressure is in the blue-colored sections. The BP1 maintains pressures above gauge pressures throughout the length of the channels.

$$\frac{\partial u}{\partial t}+\frac{\partial u^2}{\partial x}+\frac{\partial uv}{\partial y}+\frac{\partial uw}{\partial z}=-\frac{1}{\rho}\frac{\partial p}{\partial x}+\nu\left(\frac{\partial^2 u}{\partial x^2}+\frac{\partial^2 u}{\partial y^2}+\frac{\partial^2 u}{\partial z^2}\right)$$

Fig.-5: BP1 serpentine single channel, Fig. A pressure distribution along the channel length, Fig. B pressure distribution at a cross section on the outlet of the Flow field.

$$\frac{\partial u}{\partial t}+\frac{\partial u^2}{\partial x}+\frac{\partial uv}{\partial y}+\frac{\partial uw}{\partial z}=-\frac{1}{\rho}\frac{\partial p}{\partial x}+\nu\left(\frac{\partial^2 u}{\partial x^2}+\frac{\partial^2 u}{\partial y^2}+\frac{\partial^2 u}{\partial z^2}\right)$$

Fig.-6: BP2 Serpentine 3×3 single channel, Fig. A pressure distribution along channel length, and Fig. B pressure distribution across the flow field at a cross-section on the outlet.

In Fig. 6, you can find the details of CFD simulations for the flow field plate BP2 - serpentine 3×3 single channel with 9 segments. The maximum pressure drop occurs in the first row on segments 1-3. Pressure drops occur at each segment, where the entry pressure is high and the exit pressure is low. At the exit section on the BP2, the pressures drop below gauge pressure, which can cause issues to MEA and result in power reductions. From Fig. 5B & 6B, it is evident that the pressure at the exit of BP1 is higher than BP2.

$$\frac{\partial u}{\partial t}+\frac{\partial u^2}{\partial x}+\frac{\partial uv}{\partial y}+\frac{\partial uw}{\partial z}=-\frac{1}{\rho}\frac{\partial p}{\partial x}+\nu\left(\frac{\partial^2 u}{\partial x^2}+\frac{\partial^2 u}{\partial y^2}+\frac{\partial^2 u}{\partial z^2}\right)$$

Fig.-7: BP3, Serpentine 3 × 3 double channel with common inlets. Fig. A Distribution of Pressure across the flow field area from inlet to outlet, Fig. B & C pressure distribution at channels 1 & 2 at cross-section of the outlet.

Figure 7A displays the pressure distribution along the length of BP3 Serpentine 3×3 double channel, which has a common inlet and two outlets. The first and second rows are equipped with a common inlet for the double flow fields across the first and fourth segments, respectively. The flow direction for channel 1 is segments 1-2-3-6-5, while channel 2 flows through segments 4-7-8-9. BP3 has five segments for channel 1 and four segments for channel 2. As a result, the pressure drop across channel 1 is greater than that across channel 2. This is evident in Fig. 7B & 7C, where channel 2 has higher pressure than channel 1. Compared to BP2, the pressure drops are 33% better, and they are the same as that of BP1. The pressure at the exits are below gauge pressures for BP3, but the higher-pressure regions are more than those in BP1.

Fig. 8 gives the details of BP4, serpentine 3× 3 double channels with opposite inlets, this design has two channels that are exclusive to each other, and the channels have opposite inlets and outlets. The flow takes place through the inlet port through 8 sets of channels which creates 8 segments in the bipolar plate of which there are four horizontal flow fields and five vertical flow fields. Unlike BP3 where the number of segments and pressures vary for each channel, the novel BP4 has overcome the issue by having two inlets and outlets at opposite ends, thereby providing equal pressures in both channels. Fig. 8D & 8E shows the pressure distribution on the flow fields for channels 1 and 2.

$$\frac{\partial u}{\partial t}+\frac{\partial u^2}{\partial x}+\frac{\partial uv}{\partial y}+\frac{\partial uw}{\partial z}=-\frac{1}{\rho}\frac{\partial p}{\partial x}+\nu\left(\frac{\partial^2 u}{\partial x^2}+\frac{\partial^2 u}{\partial y^2}+\frac{\partial^2 u}{\partial z^2}\right)$$

Fig.-8: BP4, Novel Serpentine 3 × 3 double channel-Opposite inlets. Fig. 8A Pressure distribution across the flow field area, Fig. 8B & 8C pressure distribution at channel 1 & 2 at cross section of the outlet, Fig. 8D & 8E Distribution of pressure across Independent channels 1 & 2.

The BP4 has two channels and fluid flows are opposite in each channel, at every point the pressure across the adjacent channels are opposite. At the entry of channel 1 the pressure is high and exit of channel 2 the pressure is low therefore at this position the average pressures are to be considered since they act on the MEA. Therefore, considering the overall pressure across each segment the actual pressure acting on the MEA is the average pressure the flow across each channel. This ensures the pressure distribution across the entire Fuel cell is even and achieves the required criteria of even pressure drop across the Flow field. The pressures are well distributed here compared to the previous flow fields. Among the 9 segments, it can be found that the pressure gradually decreases slowly from the inlet to the outlet on both sides of the bipolar plate from the centreline. Fig. 8B & 8C gives the pressure distribution at a cross-section on the outlet of channels 1 and 2 respectively.

$$\frac{\partial u}{\partial t}+\frac{\partial u^2}{\partial x}+\frac{\partial uv}{\partial y}+\frac{\partial uw}{\partial z}=-\frac{1}{\rho}\frac{\partial p}{\partial x}+\nu\left(\frac{\partial^2 u}{\partial x^2}+\frac{\partial^2 u}{\partial y^2}+\frac{\partial^2 u}{\partial z^2}\right)$$

Fig.-9: BP5 Pin type bipolar plate with circular extrusions. Fig. A Pressure distribution across the length of the flow field area, Fig. B pressure distribution at cross section on the outlet

$$\frac{\partial u}{\partial t}+\frac{\partial u^2}{\partial x}+\frac{\partial uv}{\partial y}+\frac{\partial uw}{\partial z}=-\frac{1}{\rho}\frac{\partial p}{\partial x}+\nu\left(\frac{\partial^2 u}{\partial x^2}+\frac{\partial^2 u}{\partial y^2}+\frac{\partial^2 u}{\partial z^2}\right)$$

Fig.-10: BP6 Pin type bipolar plate with rectangular extrusions. Fig. A Pressure distribution across the length of the flow field area, Fig. B Pressure distribution at the cross-section of the outlet.

Fig. 9 and Fig. 10 show pressure variations in pin-type bipolar plates. While Fig. 9 is for circular pins, Fig. 10 is for rectangular pins. In both types of bipolar plates, gas enters at one corner of the Bipolar plate and emerges from the diagonally opposite end. From Fig. 9A and 10A it can be seen that in BP6 rectangular pins have better pressure distribution than BP5 circular ones, this can be seen in the figure pressures cart that at exit area the BP5 shows severe drops below zero-gauge pressures.

$$\frac{\partial u}{\partial t}+\frac{\partial u^2}{\partial x}+\frac{\partial uv}{\partial y}+\frac{\partial uw}{\partial z}=-\frac{1}{\rho}\frac{\partial p}{\partial x}+\nu\left(\frac{\partial^2 u}{\partial x^2}+\frac{\partial^2 u}{\partial y^2}+\frac{\partial^2 u}{\partial z^2}\right)$$

Fig.-11: Graph of Pressure drop across Flow Field Area, Comparison of Pressure distribution for the six bipolar plates BP1, BP2, BP3, BP4, BP5 & BP6.

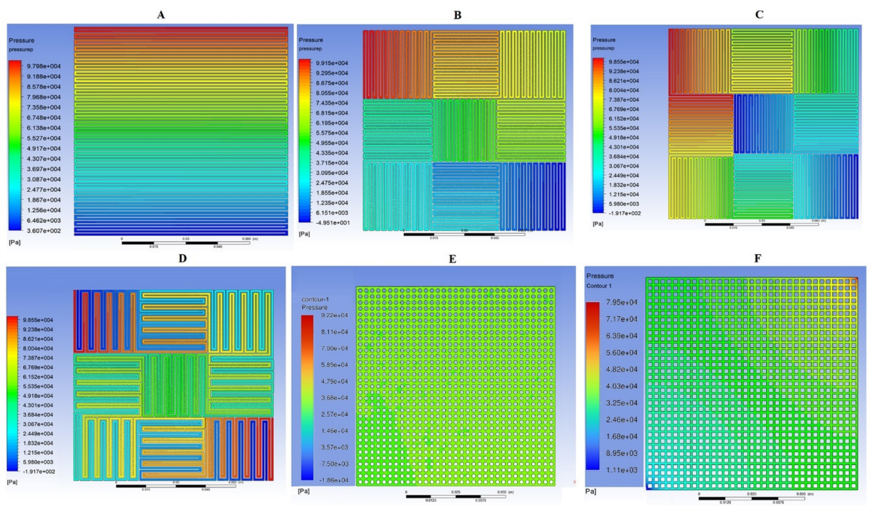

Fig.-12: Flow field plate simulation of all six plates for Comparison of Pressure distribution. Fig. A BP1, Fig. B BP2, Fig. C BP3, Fig. D BP4, Fig. E BP5, Fig. F BP6

When it comes to rectangular extrusions in Bipolar plates, the gas entering the flow field area must pass through vertical extrusions with sharp corners. This creates disturbances, which are more noticeable at the entrance due to higher pressure. As the gases flow towards the exit section of the Bipolar plates, the lower pressure prevailing there causes less disturbance. Hence, the variation in pressure in the latter half of its flow from inlet to exit produces less variation, as seen in Figure 11. A. On the other hand, the presence of circular extrusions on BP5 causes less disturbance as there is no flow separation around each extruded pin, resulting in hardly any change in pressure with Bipolar plates with circular extrusions.

Figure 11 compares the pressure drops for all six flow fields. The distance on the x-axis is across the diagonal of the flow fields, which is divided into 17 equal points, and the y-axis represents the pressure in pascals. The pressure varies between 100,000 Pa to negative pressure of 20000 Pa. From the graph, it can be seen that the novel BP4 has the least pressure drop, and the pin type with circular extensions has the maximum pressure drop below the gauge pressure. All serpentine flow fields have a constant, gradual decrease of pressure, while pins have sudden drops at the inlet and exit.

Table 3 lists the pressure values for six different gas flow channels. It is essential to maintain uniform pressure drops throughout the channels to ensure an even flow of reactants and products, as well as an equitable distribution of gases. In the bipolar plate channel of the fuel cell, gas pressures should ideally be uniform from inlet to outlet. However, the friction between channel walls, gas layers, and losses in the bends result in the pressure at the outlet being lower than the inlet, which is necessary for fluid to move from the inlet to the outlet. Different locations of the flow fields and MEA layers draw differential currents, causing variations in pressure drops. These variations can cause a drop in fuel cell performance, so flow field design should focus on minimizing pressure drops. At the bends when gas changes direction, there is a small increase in velocity and a decrease in pressure for all flow field plates (BP1 to BP4). This increase in velocity is due to the sudden expansion of gases, resulting from the larger cross-sectional area of flow at corners, creating a nozzle effect. Therefore, it is ideal to have a corner-shaped or chamfered to provide a circular path.

The values of inlet and outlet pressures for all six different gas flow channels are listed in Table 3. It is observed that as the inlet pressure increases, the outlet pressure decreases. Moreover, with 1.5 bar inlet pressure, the drop-in pressure was 21% more compared to that of 1 bar inlet pressure. It is noted that the least pressure drop has been found in the Novel BP4 (Serpentine 3×3 double channel with opposite inlets with 0.344 Pa at the outlet), as shown in graph Fig. 11. In the pin-type bipolar design, the one with circular pins has shown remarkable pressure uniformity across the surface of the GDL. The novel BP4 flow field design has opposite flows in either channel. At any given area, the flow pressures are high on one channel and low on the other channel, ensuring average pressures acting on the MEA at any given area. Hence, the pressure drop can be considered even throughout the flow field area.

CONCLUSION

In this work, six designs of fuel cell bipolar plate flow fields were simulated and studied for pressure drops and gas flow. The designs involved a combination of serpentine and pin types. Among the six flow fields, the Novel BP4 (serpentine 3×3 channel with two channels and opposite inlets and outlets) was found to be most desirable for uniform pressure drop along the channel lengths due to the differential pressures existing on the MEA which was achieved by providing more than one channel and opposite flow directions. Among the non-serpentine variants pin type with rectangular extrusions was found to produce better results in terms of maintaining uniform pressure across the flow field area. The average pressure variations across the pin-type flow field were 10% greater than that of the serpentine variants. Also, as the inlet pressure increased by 0.5 bar, the drop-in pressure was 20% at the outlet. The use of CFD simulations makes it possible to comprehend applications in various new intricate designs of the Flow Field area. Even though a Fuel Cell flow field plate can offer excellent 'even pressure drops', it may still not satisfy the required conditions of water and thermal management which is different for different flow fields, this area requires further research.

ACKNOWLEDGMENTS

This work was supported by All India Council for Technical Education (AICTE) grant funded by the Government of India (No. 8-168/FDC/RPS(Rural)/POLICY-1/2021-22) and NMAM Institute of Technology (NITTE-deemed to be university)

CONFLICT OF INTERESTS

The authors declare that there is no conflict of interest.

REFERENCES

1. B. D. Cunningham, J. Huang & D. G. Baird, Review of materials and processing methods used in the production of bipolar plates for fuel cells, International Materials Reviews, 52:1, 1-13, (2007), DOI:10.1179/174328006X102556.

2. Hossain, M. S., Shabani, B., and Cheung, C. P. Enhanced gas, flow uniformity across parallel channel cathode flow field of proton, exchange membrane fuel cells. Int. J. Hydrog. Energy 42, 5272–5283, (2017) DOI:10.1016/j.ijhydene.2016.11.042.
3. Polymer electrolyte membrane fuel cell, flow field designs and approaches for, performance enhancement, Erman Celik1 and Irfan Karagoz. Proceedings of the Institution of Mechanical Engineers, Part A: Journal of Power and Energy. (2019). DOI:10.1177/0957650919893543.
4. Al-Baghdadi. A CFD study of hygro–thermal stresses distribution in pem fuel cell during regular cell operation, renewable energy, volume 34, issue 3, (2009) doi:10.1016/j.renene.2008.05.023.
5. Anthony Anosike, Helena Loomes, Exploring the challenges of electric vehicle adoption in final mile parcel delivery, International Journal of Logistics Research and Applications, (2021).*https://doi.org/10.1080/13675567.2021.1978409.*
6. Nykvist, B., Nilsson, M. Rapidly falling costs of battery packs for electric vehicles. Nature Clim Change 5, 329–332. (2015),*https://doi.org/10.1038/nclimate2564*
7. B. Propfe, M. Redelbach, D.J. Santini, H. Friedric, Cost analysis of Plug-in Hybrid Electric Vehicles including Maintenance & Repair Costs and Resale Values, World Electr. Veh. J. 2012, 5(4), 886-895; (2012), https://doi.org/10.3390/wevj5040886.
8. Z. Chen, N. Guo, X. Li, J. Shen, R. Xiao, S. Li, Battery Pack Grouping and Capacity Improvement for Electric Vehicles Based on a Genetic Algorithm (Energies, vol 10, issue 4)., 10(4), 439; (2017), https://doi.org/10.3390/en10040439.
9. Richard K. Lattanzio, Corrie E. Clark, Environmental Effects of Battery Electric and Internal Combustion Engine Vehicles, Congressional Research Service CRS Report. (2020)
10. Abha Bharti, Rajalakshmi N atarajan, Proton exchange membrane testing and diagnostics, PEM Fuel Cells, 10.1016/B978-0-12-823708-3.00007-9, (137-171), (2022), DOI:10.1016/b978-0-12-823708-3.00007-9
11. TolgaTaner, The novel and innovative design with using H2 fuel of PEM fuel cell: Efficiency of thermodynamic analyze, Fuel, Volume 302, 121109, (2021) *https://doi.org/10.1016/j.fuel.2021.121109.*
12. Vincenzo Liso, Samuel Simon Araya, Thermodynamics and operating conditions for proton exchange membrane fuel cells, PEM Fuel Cells Fundamentals, Advanced Technologies, and Practical Application, Pages 123-136. (2022) DOI: 10.1016/B978-0-12-823708-3.00014-6
13. 13Wilberforce, T.; Ijaodola, O.; Emmanuel, O.; Thompson, J.; Olabi, A.G.; Abdelkareem, M.A.; Sayed, E.T.; Elsaid, K.; Maghrabie, H.M. Optimization of Fuel Cell Performance Using Computational Fluid Dynamics. Membranes, 11, 146. (2021)*https://doi.org/10.3390/membranes11020146*
14. Li, H., Tang, Y.,Wang, Z., Shi, Z.,Wu, S., Song, D., et al. (2008). A review of water flooding issues in the proton exchange membrane fuel cell. J. Power Sources 178,103–117. (2007) DOI: 10.1016/j.jpowsour.2007.12.068
15. Hussaini, I. S., and Wang, C. Visualization and quantification of cathode channel flooding in PEM fuel cells. J. Power Sources 187, 444–451. (2009) DOI: 10.1016/j.jpowsour.2008.11.030
16. Youcef Kerkoub, Ahmed Benzaoui et al. Energy Conversion and Management, Volume 174, 15 October, Channel to rib width ratio influence with various flow field designs on performance of PEM fuel cell, (2018), https://doi.org/10.1016/j.enconman.2018.08.041.
17. Ata Chitsaz, Thermodynamic and exergoeconomic analyses of a proton exchange membrane fuel cell (PEMFC) system and the feasibility evaluation of integrating with a proton exchange membrane electrolyzer (PEME), Energy Conversion and Management 186:487-499. (2019) DOI:10.1016/j.enconman.2019.03.004.
18. Hassan Kargar-Pishbijari, Seyed Jamal Hosseinipour. A novel method for manufacturing microchannels of metallic bipolar plate fuel cell by the hot metal gas forming process, val10.1016/j.jmapro.2020.04.040Journal of Manufacturing Processes. (2019) DOI:10.3389/fenrg.2020.00013.
19. Marco Sauermoser, Natalya Kizilova, Flow Field Patterns for Proton Exchange Membrane Fuel Cells, Frontiers in Energy Research.*https://doi.org/10.3389/fenrg.2020.00013.* (2020)
20. H. Kahraman, A. Coban. Performance Improvement of a Single PEM Fuel Cell Using an In-

novative Flow Field Design Methodology, Arabian Journal for Science and Engineering. (2020), DOI:10.1007/s13369-020-04368-y

21. Spernjak, D., Prasad. In situ comparison of water content and dynamics in parallel, single-serpentine, and interdigitated flow fields of polymer electrolyte membrane fuel cells. J. Power Sources. (2010), DOI: 10.1016/j.jpowsour.2009.12.031
22. Ghanbariana, M.J. Kermanib, Polymer electrolyte membrane fuel cell flow field design criteria – Application to parallel serpentine flow patterns, Energy Conversion and Management. (2018) doi:10.1016/j.enconman.2018.04.018
23. Guo, N., Leu, m.c., & wu, m. bio-inspired design of bipolar plate flow fields for polymer electrolyte membrane fuel cells. proceedings of, international SFF symposium (2011)
24. Jean-Paul Kone et all. The Journal of Computational Multiphase Flows 2017, Vol. 9(1) 3–sagepub.co.uk.journals.sagepub.com/home/cmf(2017)DOI: 10.1177/1757482X17692341
25. Li, X., and Sabir, I. (2005). Review of bipolar plates in PEM fuel cells: flow field designs. Int. J. Hydrog. Energy 30, 359–371. (2004) DOI: 10.1016/j.ijhydene.
26. Marco Sauermoser, Natalya Kizilova, Flow Field Patterns for Proton Exchange Membrane Fuel Cells, Frontiers in Energy Research. (2020), DOI: 10.1177/1757482X17692341.
27. Fahim, K.H., Alfayydh, E.M., & Dhahad, H.A. Effect of Geometric Design of the Flow Fields Plat on the Performance of A PEM Fuel Cell: A Review. University of Technology, Iraq, 34. (2017) Corpus ID: 212575175.
28. Justo Lobato, Pablo Cañizares,Study of flow channel geometry using current distribution measurement in a high temperature polymer electrolyte membrane fuel cell, Journal of Power Sources, 2011, https://doi.org/10.1016/j.jpowsour.
29. Lim, B. H., Majlan, E. H., Daud, Numerical analysis of modified parallel flow field designs for fuel cells. Int. J. Hydrog. Energy 42, 9210–9218. (2017). DOI:10.1016/j.ijhydene.2016.03.189
30. Guo, N., Leu, M. C., and Koylu, U. O. Network based optimization model, for pin-type flow field of polymer electrolyte membrane fuel cell. Int. J. Hydrog. Energy 38, 6750–6761. (2013). DOI: 10.1016/j.ijhydene.2013.03.066.
31. Ascencio, C.E., Guerrero, A.H., Vargas, J.A., & Rubio-Arana, C. Three-Dimensional Numerical Prediction of Current Density for a Constructal Theory-Based Flow Field Pattern. Proceedings of the ASME 2007 International Mechanical Engineering Congress and Exposition. (2007). DOI:10.1115/IMECE2007-42449.
32. Ozden, A., Ercelik, M., Ouellette, D., Colpan, C. O., Ganjehsarabi, H., and Hamdullahpur, F. Designing, modeling and performance investigation of bio-inspired flow field based DMFCs. Int. J. Hydrog. Energy 42, 21546–21558. (2017) DOI: 10.1016/j.ijhydene.2017.01.007
33. Gao Y. Type of fuel cell bipolar plates constructed with multiple pass flow channels that contract, expand, deflect and split reactant flows for improving reactant flow distribution, diffusion and water management. (2009) Patent application 20090214929, USA,
34. Fan L, Niu Z, Zhang G, et al. Optimization design of the cathode flow channel for proton exchange membrane fuel cells. energy convers manag;171:1813–1821.(2018) DOI:10.1016/j.enconman.2018.06.111.
35. D.H. Jeon, S. Greenway, S. Shimpalee, J.W. Van Zee, The effect of serpentine flow-field designs on PEM fuel cell performance International Journal of Hydrogen Energy, 33, pp. 1052-1066. (2008)
36. A. Iranzo, M. Muñoz, F. Rosa, J. Pino Numerical model for the performance prediction of a PEM fuel cell. Model results and experimental validation International Journal of Hydrogen Energy, 35, pp. 11533-11550 A. (2010),
37. Iranzo, M. Muñoz, J. Pino, Update on numerical model for the performance prediction of a PEM fuel cell International Journal of Hydrogen Energy, 36 pp. 9123-9127 (2011)
38. Ji, M., and Wei, Z. A review of water management in polymer electrolyte membrane fuel cells. Energies 2, 1057–1106. (2009). DOI:10.3390/en20401057.